Short-pulse terahertz radiation from high-intensity-laser-produced plasmas

H. Hamster, A. Sullivan, S. Gordon, and R. W. Falcone
Department of Physics, University of California at Berkeley, Berkeley, California 94720
(Received 29 July 1993)

The interaction between high-intensity, ultrashort laser pulses and plasmas leads to the emission of coherent, short-pulse radiation at terahertz frequencies. In this work we discuss a model for this effect and its experimental realization. Our measurements constitute the direct observation of laser-induced wake fields. From gas-density targets, resonant enhancement of the terahertz emission is observed if the plasma frequency is close to the inverse pulse length of the exciting laser pulse. At higher plasma densities, the emission of subpicosecond, unipolar electromagnetic pulses is observed. With the use of solid density targets, emission of more than 0.5 μJ of far-infrared-radiation energy was measured. Simultaneous emission of MeV x rays and 0.6-MeV electrons was observed and correlated with the terahertz emission. This indicates that the radiative processes in such plasmas are driven by ponderomotively induced space-charge fields in excess of 10^8 V/cm.

PACS number(s): 52.40.Nk, 42.65.Re, 52.25.Rv, 52.35.Mw

The interaction of intense laser light with plasmas is a complex process which requires a sophisticated theoretical treatment [1–6]. Experimental observations are of great importance to enhance our understanding of these phenomena. In this paper we report the observation of electromagnetic transients that result from such interactions. The interpretation of these measurements allows a better understanding of the underlying plasma dynamics. Our research illuminates the mechanism which leads to the generation of wake fields, energetic electrons, x rays and terahertz radiation from laser-produced plasmas.

Plasmas created by high-intensity laser pulses with subpicosecond duration have received considerable attention as sources of radiation. The observed emission includes radiation at very high harmonics of the laser frequency [7,8], x-ray bursts of subpicosecond duration [9], and the generation of hard x rays with energies of greater than 1 MeV [10]. At the low-energy end of the electromagnetic spectrum, a strong emission of coherent far-infrared radiation (FIR) at terahertz frequencies has been predicted [11]. This radiation arises from the rapid development of space-charge fields in such plasmas. We have recently reported an observation of this effect [12] and in this paper we give a more detailed account of those measurements.

The generation of strong electric and magnetic fields by laser-induced plasmas has been considered before. The creation of magnetic fields with megagauss strength in the focus of subnanosecond laser pulses was observed in the 1970s [13,14]. Electrical fields greater than 10^8 V/cm have been predicted in the context of plasma-wave accelerators [2] and for the interaction of high-intensity short-pulse lasers with plasmas [3]. Magnetic fields up to 10^9 G were calculated for the interaction of intense short-pulse lasers with solid-density plasmas [4,5]. Electric fields of up to 10^7 V/cm have been measured in experiments involving plasma-wave accelerators [15]. Our experiments allow a comparison with this previous work by measuring the time derivative of these fields in the far field.

Terahertz radiation results from the interaction of femtosecond laser pulses with matter through a variety of different mechanisms. These employ electro-optic crystals [16], photoconductive switches and antennas [17,18], or large-area semiconductor wafers [19,20]. Pulse energies of up to 0.8 μJ have been demonstrated by using a biased Ga-As wafer [21].

In our experiment the mechanism of pulse generation involves ponderomotive forces generated in the focus of an intense femtosecond laser pulse. These forces create a large density difference between ionic and electronic charges if the pulse length is short enough to inertially confine the ions [3,6]. This results in a powerful electromagnetic transient. Using Poisson's equation and Larmor's formula we estimate that the emitted FIR power P (in MW) is given by [11,22]

$$P \approx \frac{1}{7}\left[\frac{W}{R_0}\right]^2\left[\frac{\lambda}{\tau}\right]^4, \tag{1}$$

where W is the laser energy in J, R_0 is the $1/e^2$ radius of the focused beam in μm, λ is the laser wavelength in μm, and τ is the pulse length in ps. For a pulse energy of 1 J, 1-μm beam radius, 0.1-ps pulse length, and 1-μm laser wavelength, we expect peak powers in excess of 1 GW.

In order to estimate the FIR emission in a more rigorous fashion, we have employed a linearized hydrodynamic model for the plasma dynamics. By calculating the spatial and temporal dependence of the charge density and acceleration within the focal region we are able to compute the far-field radiation pattern. In particular, we require the electron density $n(r,z,t)$ and acceleration $\mathbf{a}(r,z,t)$ as a function of time t and cylindrical coordinates r and z. We assume radial symmetry around the direction of propagation $\hat{z}$ and model the electron fluid as cold, i.e., the thermal pressure $p = nk_B T_e$ is assumed to be

small compared to the ponderomotive pressure $nU_{\rm pon}$. k_B is the Boltzmann constant and T_e the electron temperature; the ponderomotive energy $U_{\rm pon}$ is defined in Ref. [23]. The cold-fluid approximation is justified since plasmas produced by short-pulse lasers tend to have temperatures below 10^3 eV [24,25] while the ponderomotive energies for our experimental conditions are on the order of 10^5 eV. Under these conditions, the dynamical equations of motion for the electron fluid [26] may be linearized and decoupled to yield simple harmonic oscillator equations for the density n, velocity $\mathbf{v}$, and a low-frequency electric field $\mathbf{E}$ which arises from charge separation [27]. We solved this system of harmonic oscillator equations for a realistic beam profile by using the method of variation of constants. We choose a temporally and spatially Gaussian pulse envelope while considering the natural divergence of the Gaussian mode. The ponderomotive potential used is given by

$$U_{\rm pon}(r,z,t)=U_0\frac{R_0^2}{R_0^2+z^2\kappa^2}\exp\left[-\frac{r^2}{R_0^2+z^2\kappa^2}\right]\times\exp\left[-\frac{(z/v_g-t)^2}{\tau_0^2}\right]. \quad (2)$$

Here U_0 is the ponderomotive energy at the peak intensity of the laser, v_g is the group velocity of the pulse in the plasma, $\kappa=\lambda/(\sqrt{2}\pi R_0)$ is a constant relating to the divergence of the beam, and the time τ_0 is the $1/e^2$ half-width of the pulse. The model can be solved in a closed form and the resulting analytical expressions for n, $\mathbf{v}$, and $\mathbf{E}$ are given in terms of the error function with a complex argument [22]. The time derivative of the resulting current is summed numerically over the excitation volume at retarded times in order to calculate the far-field radiation pattern. Note that we employ an expression which contains all orders in a multipole expansion [26].

The terahertz radiation will experience losses while propagating out of the laser-produced plasma since the plasma is overcritical to electromagnetic waves with frequencies below the plasma frequency ω_p. Due to the small spatial extent of the plasma these losses are estimated to be small and are therefore not further considered.

Figure 1 gives examples of our calculations. The emitted FIR power is shown versus view angle and time. The results of these calculations may be summarized as follows. The peak of the emission is in the forward direction with respect to the beam propagation. A strong resonant enhancement of the signal is observed for $\omega_p\tau_0=2$. In this density regime ($n\approx 2\times 10^{17}$ cm^{-3} for $\tau_0\approx 0.1$ ps) one expects the emission of radiation over many cycles of the plasma oscillation. This is shown in Fig. 1(a) for a plasma frequency $\omega_p/2\pi$ of 4.6 THz. We note that the damping of the plasma oscillations on a time scale of a few picoseconds due to electron-ion collision can be ruled

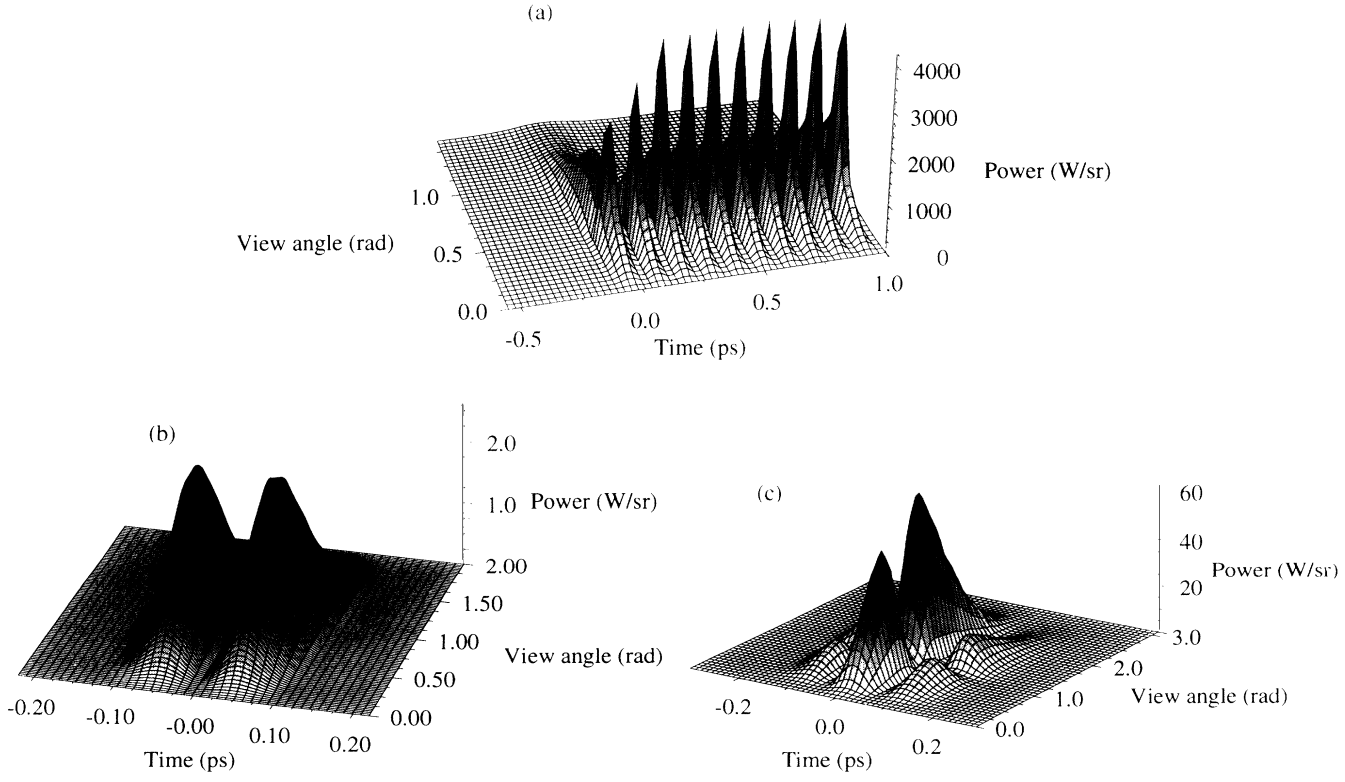

FIG. 1. Calculated radiation pattern. The vertical axis denotes power (W/sr); the bottom axes are time (ps) and view angle (rad) with respect to the beam propagation direction. The calculations are for a pulse length of 120 fs FWHM, 50-mJ pulse energy, and a beam diameter of 3 μm. (a) Resonant plasma response when the electron density is 2.5×10^{17} cm^{-3}. (b) Nonresonant response at a density of 10^{19} cm^{-3}. (c) FIR signal due to $\mathbf{J}^{\rm NL}$ at a density of 10^{19} cm^{-3}.

out; a dephasing time of less than 2 ps requires a plasma temperature below 0.5 eV [28]. This seems too low for this type of laser-produced plasma [24,25].

Figure 1(b) shows the case of nonresonant excitation of plasma at a density of 10^{19} cm^{-3}. The peak power remains relatively low while the pulse shape is essentially given by the derivative of the exciting optical pulse. Note that there is a dependence of the spatial emission pattern on the spot size of the focused laser beam. A smaller beam leads to a shift of the emission maximum in a direction perpendicular to the laser propagation.

The radiation discussed so far arises solely from a *time-averaged* driving force. There will be an additional radiative contribution which originates from the oscillation of the plasma at frequencies of $\omega \pm \Delta\omega$, where ω is the carrier frequency and $\Delta\omega$ is the bandwidth of the laser pulse. The frequencies components will mix if the plasma is inhomogeneous, i.e., $\nabla n \neq 0$. This nonlinear current has been calculated before for the case of second-harmonic generation in a plasma [29]. In a very similar fashion we estimate the leading contribution due to this effect to be given by [22]

$$\mathbf{J}^{\mathrm{NL}}(\Delta\omega,\omega,-\omega)=\frac{4\pi e^3}{\omega^3 m_e^2 c}\left[\frac{1}{1-(\omega_p/\omega)^2}\right] \times I(\nabla n\cdot\mathbf{e}_{\mathrm{pol}})\mathbf{e}_{\mathrm{pol}} . \quad (3)$$

$\mathbf{e}_{\mathrm{pol}}$ is the polarization vector of the exciting electromagnetic field, I is the laser intensity, and e and m_e are the electron charge and mass. Note that $\mathbf{J}^{\mathrm{NL}}$ is proportional to I and will only implicitly depend on the ponderomotive force through ∇n. We compute the far-field radiation pattern by integrating $d\mathbf{J}^{\mathrm{NL}}/dt$ over the excitation volume. ∇n is obtained from the hydrodynamic model. The result of one such calculation is shown Fig. 1(c) for $n=10^{19}$ cm^{-3} and $I=5\times10^{18}$ W/cm^2.

In order to measure these effects, we used a terawatt laser system [30] capable of producing intensities up to 10^{19} W/cm^2. We achieve a pulse length of typically 120 fs and an energy of up to 0.5 J at 0.8-μm wavelength. The beam was focused with a 5-cm focal length off-axis paraboloidal reflector to a size of approximately 3.5×2.5 μm.[2] At a laser repetition rate of 10 Hz, experiments were performed with a pulse energy of 20–50 mJ. At higher energies the repetition rate was limited to several shots per minute.

The first series of experiments was performed in a chamber filled with gas of pressures up to 10^5 Pa. The emitted radiation was collected by using a short-focal-length off-axis paraboloidal mirror with $f/0.5$. A liquid-helium-cooled bolometer was used in conjunction with a Fourier-transform spectrometer to characterize the emitted FIR [31]. Care was taken in order to ensure that the optical path leading into the detector was free of water vapor. Sheets of thin black polyethylene prevented laser light from reaching the detector.

Figure 2(a) shows the detected terahertz signal as a function of pressure as well as our model calculation. The absolute energy scale on the right-hand side of the graph is only accurate within a factor of 2 due to the uncertainty of the optical throughput of our detection system. As expected, we observe a strong resonant enhancement of the radiation if the plasma frequency is close to the inverse pulse length of the laser. However, our linearized model fails to predict accurately the behavior at high pressures. A nonperturbative treatment for the plasma response in this pressure regime appears to be necessary. Figure 2(b) indicates the different contributions to the calculated signal. We believe the plateau around 6000 Pa is due to an artifact of the calculation [22].

The interferograms reveal that the strong signal around 400 Pa is indeed due to the oscillation of the plasma at the plasma frequency. We observe several cycles of radiation extending over a period of about 2 ps [Fig. 3(a)]. Assuming that the damping of the waves is due to electron-ion collisions in a thermal plasma, we infer an unreasonably low temperature of only 0.5 eV. However, we estimate that the radiative damping is considerable. Modeling the plasma as a column with a diameter of 5 μm and a length of $\approx$50 μm, and assuming the electron density in the column is lowered by 10^{17} cm^{-3} from its unperturbed value, we estimate the electrostatic self-energy to be several nanojoules. The measured radiative yield is around 1 nJ. In addition, other nonlinear damping mechanisms such as wave breaking [32] will have to be considered.

The frequency of the emission of the resonant signal is both tunable with density and close to the bulk plasma frequency as shown in Fig. 4. This observation is in-

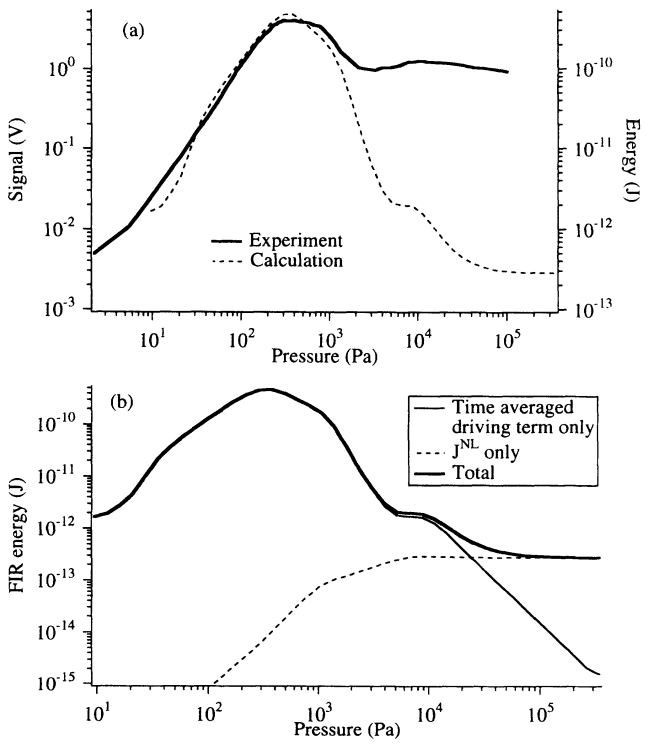

FIG. 2. (a) Observed FIR emission for He gas as a function of pressure in comparison with calculations assuming a 140-fs, 50-mJ laser pulse. (b) Calculation of different contributions to the FIR signal. Shown are the contributions due to the time-averaged source term, due to $\mathbf{J}^{\mathrm{NL}}$ and the sum of both signals.

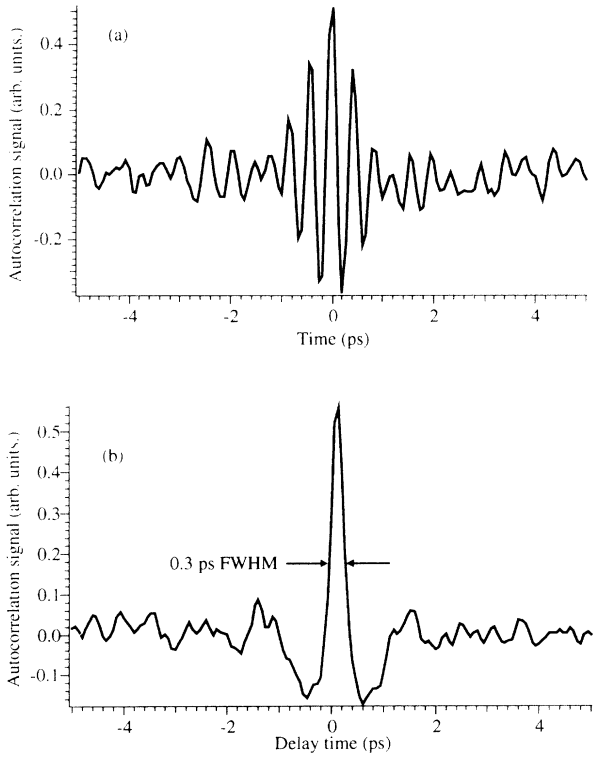

FIG. 3. Autocorrelation of FIR signal in He for 120-fs, 50-mJ pulses. (a) Resonant excitation at an electron density of 7×10^{16} cm^{-3}. (b) Nonresonant excitation at a density of 2×10^{19} cm^{-3}.

teresting since the size and shape of the plasma are expected to lead to a deviation from the bulk plasma frequency.

At the highest density a new peak in the spectrum appears which is centered around 1.5 THz. The location of the peak remains essentially unchanged for all densities above 10^{18} cm^{-3} (Fig. 5) and is also independent of the gas in which the experiment was carried out (He, Ar, N, air). The autocorrelation signal of such a pulse is shown

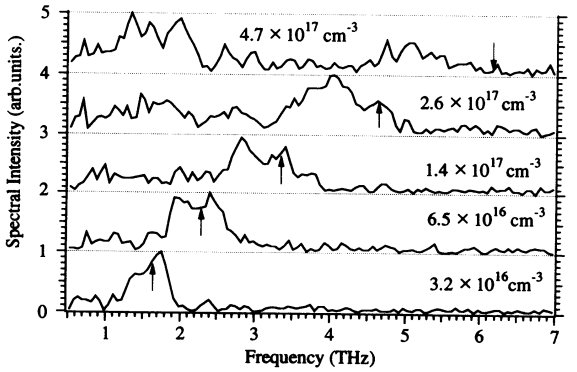

FIG. 4. Spectra for a resonant excitation of the plasma where $\omega_p\tau_0\approx2$. The arrows indicate the plasma frequency $\omega_p/2\pi$ at each density. Note the emerging nonresonant signal around 1.5 THz at the highest densities. Data is for a He gas and 120-fs, 50-mJ laser pulses.

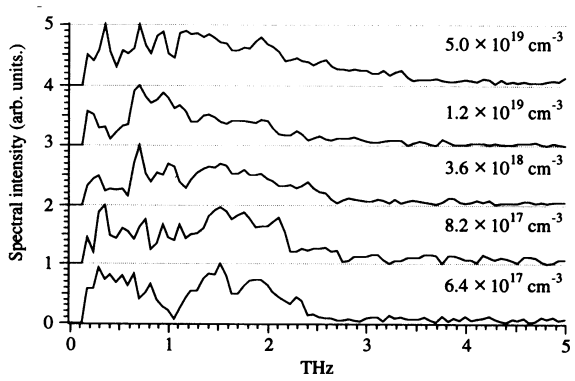

FIG. 5. Spectra for nonresonant excitation of the plasma, i.e., $\omega_p\tau_0\gg2$. Data is for a He gas target and 120-fs, 50-mJ laser pulses.

in Fig. 3(b) and has a full width at half-maximum (FWHM) of 0.3 ps. It shows a pulse which is dominantly unipolar. The pulse shape resembles the temporal characteristics calculated in Fig. 1(c), indicating that this signal may be due to $\mathbf{J}^{\mathrm{NL}}$. The signal is p polarized as expected from Eq. (3). The fact that we fail to predict the signal strength correctly at this pressure is likely due to the breakdown of the linearized model. We found that the strength of the nonresonant signal was dependent on the target gas. In Ar, the nonresonant emission peaks at a pressure of 6500 Pa and is twice as strong as the resonant signal observed at low pressures (Fig. 6). The polarization of the signal is also pressure dependent and changes direction at intermediate pressures. At very high pressures ($>1.5\times10^4$ Pa) the signal becomes depolarized. This is probably caused by the severe beam distortion and breakup that is observed at high densities [33]. We believe the high plasma density in case of the Ar target is significant for an explanation of the observed differences with our experiments in He.

The first-order autocorrelation trace obtained with a Michelson interferometer alone does not provide a measure of the pulse length. Interferograms similar to Fig. 3(b) may be obtained from a broad-band thermal source.

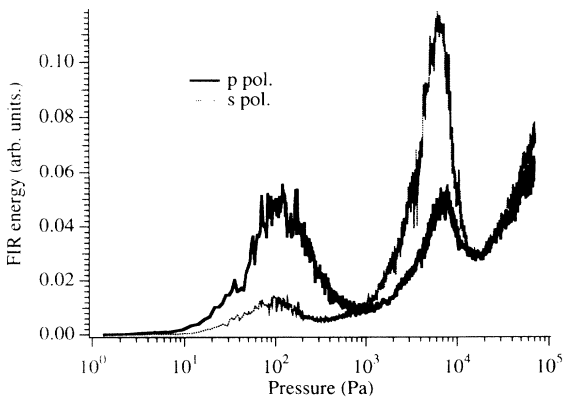

FIG. 6. Observed terahertz emission from an Ar plasma vs pressure for s and p polarization. The laser pulse length was 120 fs and the energy 50 mJ.

However, we estimate the emission due to thermal bremsstrahlung from the plasma to be several orders of magnitude smaller than the observed signal levels [22,34]. In addition, we performed a direct measurement of the pulse in the time domain. The terahertz radiation was transmitted through a semi-insulating Ga-As wafer which functioned as a transient mirror following illumination with femtosecond optical radiation [21,35]. We confirmed that for the case of nonresonant excitation all of the FIR was contained in a time interval of less than 0.8 ps (10–90 % points, Fig. 7). The resonant excitation signal was emitted over a period of 1.7 ps. The fall time of the nonresonant signal was independent of the target gas and constant over a wide pressure range. We were not able to distinguish individual cycles of radiation for the case of resonant emission. This indicates that our measurement of a 0.8-ps fall time was limited by the time resolution of the technique.

We confirmed qualitatively that the main peak of the terahertz emission was directed forward, about 60° with respect to the direction of beam propagation. No radiation was detected in the backward direction. However, we were not able to make a quantitative comparison with theory because of the large collection angle of the off-axis paraboloidal mirror.

In a second set of experiments we investigated the emission of terahertz radiation from a solid target. The *p*-polarized laser light was incident on the target at $\approx 60°$ with respect to normal. Al-coated glass slides were used as targets. The target chamber was filled with dry nitrogen of ≈ 2500-Pa pressure in order to protect the focusing mirror from debris. This had no noticeable effect on the emission. Since the radiation is emitted from a spatially fixed interface and not from a moving focus, we expect the emission pattern to be different from the ones shown in Fig. 1. For the case of normal incidence, the main emission is calculated to be in the backward direction $\approx 50°$ off normal [11,22]. In the experiment, we found the emission to be at a maximum in the direction of specular forward reflection. The radiation was found to be *p* polarized. The signal in the direction opposite to the incident laser beam was two orders of magnitude smaller. By using a pyroelectric detector in conjunction with a collection cone and a light pipe, we observe 0.5 μJ of FIR emitted into a solid angle of 1.5 sr at an optical pulse energy of 200 mJ. Due to coupling losses and the insufficient absorption of the detector element we estimate the actual radiative yield to be a factor of 3 higher. Assuming a pulse length of 0.5 ps we infer a peak FIR power of greater than 1 MW.

We observe that each laser pulse must be preceded by a small amount of amplified spontaneous emission (ASE) in order to optimize the emission of FIR. Our main pulse is accompanied by a 5-ns ASE pedestal with an energy contrast to the main pulse of 4×10^3. By using glass saturable absorber filters, we improved this contrast ratio to 4×10^5. However, the emitted FIR dropped by a factor of 10 when the saturable absorber was inserted. The total amount of emitted FIR scales linearly with the incident laser energy as shown in Fig. 8. We observe large fluctuations of the FIR signal on a shot-to-shot basis which are *not* correlated to fluctuations in the second harmonic of the laser from a potassium dihydrogen phosphate (KDP) crystal. We were also not able to clearly relate these fluctuations to surface inhomogeneities or to vibrations of the target mount.

Along with the terahertz emission we observe a hard-x-ray signal. The x rays penetrate the 5-mm-thick steel wall of the target chamber, which provides a low-energy cutoff of 0.1 MeV. They are detected with a 7.5-cm-diameter NaI detector which is kept at 3-m distance and 70° off normal from the target. We observe the same signatures for the hard-x-ray emission as reported previously [10], e.g., the strongest x-ray yield is observed when a strong scatter of light from the $\frac{3}{2}$ harmonic of the laser occurs.

The x-ray and FIR emission occur simultaneously. Figure 9(a) shows the x-ray signal on the NaI detector versus the FIR signal for 16 000 shots. Both emissions are correlated on a shot-to-shot basis by a power law with an exponent of 0.7.

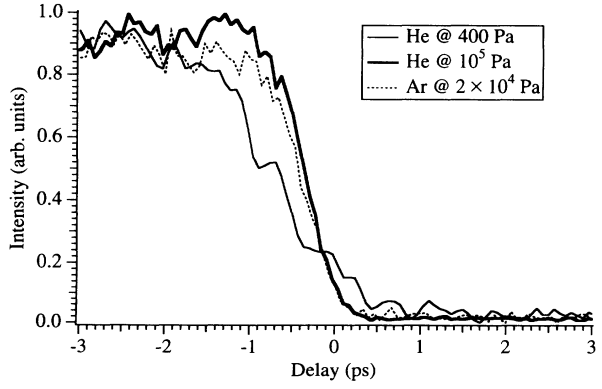

FIG. 7. Transmission through an optically gated Ga-As wafer. 10–90 % fall times are 0.8 ps for the case of nonresonant excitation in Ar or He and 1.7 ps for the resonant signal for He at a pressure of 400 Pa.

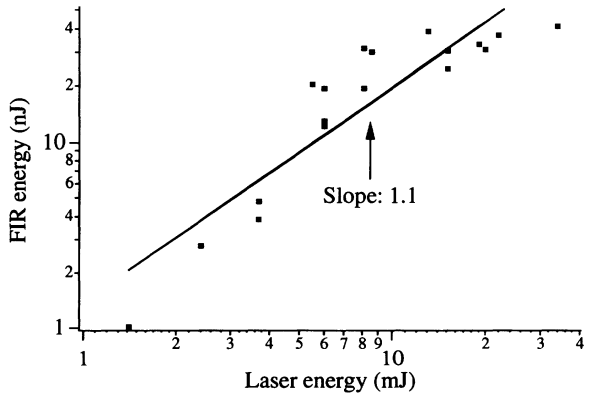

FIG. 8. Dependence of the terahertz emission from a solid target on the laser energy. Each point represents an average of 1000 laser shots. The laser-pulse energy was attenuated with neutral density filters. A dependence between the laser energy and FIR yield by a power law with an exponent of 1.1 is derived from a least-squares fit.

In addition, we detected the emission of energetic electrons from the plasma. We used a 5-mm-thick piece of BC408 scintillator plastic to detect the electrons. Before reaching the detector, the electrons had to penetrate a 0.2-mm-thick sheet of black polyethylene which served as a vacuum window. By using a 5000-G Sm:Co magnet we verified that the signal was indeed due to electrons and not x rays. The contrast ratio between electron and x-ray signal on the detector was determined to be greater than 10^3. Al sheets of varying thickness were used to determine the electron energy since the stopping powers for energetic electrons in different materials are well documented [36]. We estimate that the bulk of the electrons had an energy of 0.6 MeV at a laser intensity of 1.6×10^{18} W/cm^2. This energy is approximately four times larger than predicted by computer simulations [4]. The ponderomotive energy of the focused laser is 0.1 MeV, but we believe that the electrons originate close to the critical surface where the electric field is strongly enhanced [37]. This is supported by the observation that strong emission is detected only if the target is prepulsed with energy in excess of about 1 μJ. Simultaneously, we observe light at the $\frac{3}{2}$ harmonic of the laser which comes from a region with quarter critical density [1].

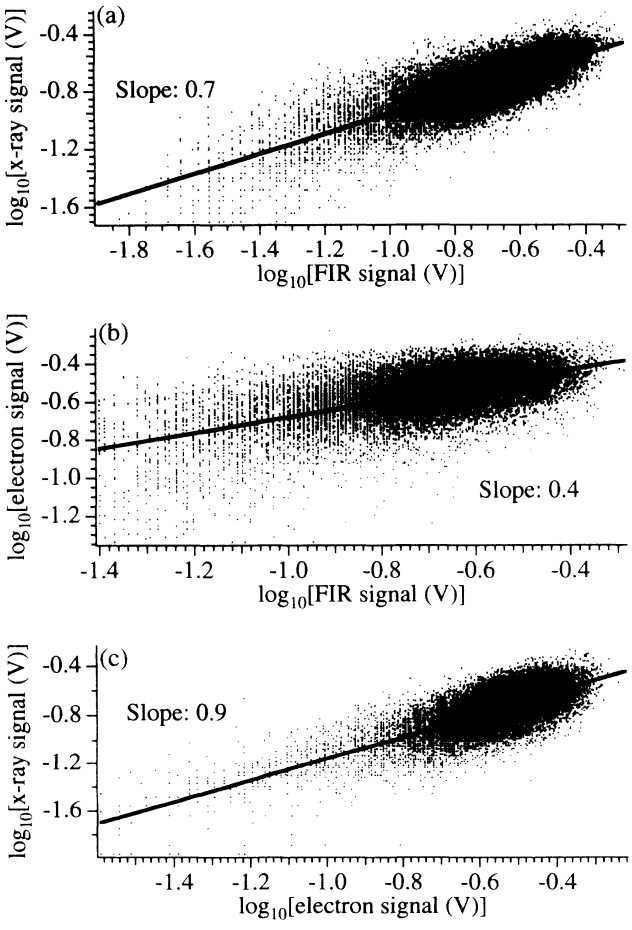

FIG. 9. Correlation between hot-electron, x-ray, and terahertz emission from a solid target. Each graph shows the signal for 16000 laser shots. The slopes are obtained from a least-squares fit. (a) FIR signal vs x-ray signal. (b) Electron signal vs FIR signal. (c) X-ray signal vs electron signal.

The electron signal is correlated to the terahertz emission as shown in Fig. 9(b). We compute a power law with an exponent of 0.4. The electron emission is also related to the x-ray signal as shown in Fig. 9(c). The x-ray yield goes as the 0.9 power of the electronic signal.

One may try to understand these scalings in the following way. The simultaneous occurrence of strong x-ray, β, and FIR emissions indicates that the radiative processes are driven by ponderomotively induced space-charge fields at the critical surface. The fields which give rise to the emission of terahertz radiation accelerate the electrons, which then in turn produce energetic x-rays via bremsstrahlung in the target substrate. The scaling of such a process is well known for x-ray tubes and is given by $P_x \propto W^2 I$ [38], where W is the electron energy, I the current, and P_x the emitted x-ray power. However, we fail to explain the observed power laws for the x-ray yield on the basis of this simple analogy. We may assume that the current I is constant since it will be determined by the total amount of excluded charges in the high-intensity region. This number is directly related to the ponderomotive energy which fluctuates little as indicated by the reference signal from the KDP crystal. Since W will be proportional to the low-frequency electric field E, and the emitted FIR power $P_{\rm FIR}$ will be proportional to E^2, we expect the x-ray yield to go linear with the FIR signal. We observe $P_x \propto (P_{\rm FIR})^{0.7}$. The electronic signal P_e is proportional to WI, and hence we expect $P_x \propto (P_e)^{2.0}$, which contrasts the observed value of 0.9. However, the relation between FIR and electron signal is expected to be $P_e \propto (P_{\rm FIR})^{0.5}$, which compares well to the experimentally observed exponent of 0.4.

It is also interesting to compare the radiative yields for all three types of radiation. Assuming that the electrons emitted from the plasma have an average energy of 0.6 MeV and are isotropically distributed, we estimate that 2×10^9 electrons are emitted by the plasma per shot at a pulse energy of 20 mJ. The NaI detector was calibrated with a 100-μCi source of Cs^{137} in place of the laser focus. This allowed us to estimate the relative number of Compton events. Assuming a photon energy of 0.2 MeV, which is the average energy for a photon produced via bremsstrahlung by a 0.6-MeV electron [39], we estimate that a total of 10^7 x rays are produced per shot. The electron-to-x-ray energy conversion is thus 0.2%. This compares well with calculated bremsstrahlung yield of 0.4% for 0.6-MeV electrons in glass [36].

We can make an estimate for the strength of the low-frequency electric field in the focal region. Assuming that the electrons are accelerated over a distance of a few micrometers, we readily infer a field strength on the order of 10^9 V/cm from the observation of 0.6-MeV electrons. At the same time we infer a field strength on the order of 10^8 V/cm from the observation of terahertz radiation with a peak power of several megawatts emerging from a spot a few micrometers in size. This corresponds to a strength of the magnetic field of the electromagnetic wave of $\approx 3\times10^5$ G. The discrepancy in field strength by a factor of 10 between both estimates may be reconciled

by considering that there will be a coupling loss since the FIR has to penetrate a dense plasma which is overcritical for terahertz radiation. We note that key to inferring these high fields is the assumption that the radiation emerges from a spot of less than 10 μm in diameter. This is well justified since all length scales entering the problem, i.e., the beam diameter, the attenuation length of the laser field and the plasma scale length, are smaller than or equal to a few micrometers. We also note that the peak electric field of the laser is about 3×10^{10} V/cm for a power density of 1×10^{18} W/cm^2.

In conclusion, we have demonstrated that short-pulse-laser-produced plasmas are a novel and powerful source for the generation of short-pulse terahertz radiation; we have demonstrated peak powers in excess of 1 MW. We also report the *direct* observation of laser-induced wake fields. The measurement of electromagnetic pulses in laser-plasma interactions may contribute as a diagnostic tool to the realization of laser-based particle accelerators. Further, we have shown that the emission of FIR is strongly correlated with the production of x rays and electrons of MeV energies. This may allow novel experiments with ultrafast-time resolution, cross-correlating beams that span the electromagnetic spectrum from meV to MeV energies.

It is a pleasure to acknowledge help from and fruitful discussions with A. Belkacem, W. Holmes, W. Leemans, M. Nahum, S. Verghese, and W. White. H. H. was supported by the Studienstiftung des deutschen Volkes. This work was supported by the U.S. Air Force Office of Scientific Research and through a collaboration with Lawrence Livermore National Laboratory under Contract No. W-7405-ENG-48.

[1] W. L. Kruer, *The Physics of Laser Plasma Interaction* (Addison-Wesley, Reading, MA, 1988).
[2] C. Joshi *et al.*, Nature **311**, 525 (1984).
[3] P. Sprangle, E. Esarey, and A. Ting, Phys. Rev. Lett. **64**, 2011 (1990).
[4] S. C. Wilks *et al.*, Phys. Rev. Lett. **69**, 1383 (1992).
[5] R. N. Sudan, Phys. Rev. Lett. **70**, 3075 (1993).
[6] G. Z. Sun *et al.*, Phys. Fluids **30**, 526 (1987).
[7] J. J. Macklin, J. D. Kmetec, and C. L. Gordon, Phys. Rev. Lett. **70**, 766 (1993).
[8] A. L'Huillier and P. Balcou, Phys. Rev. Lett. **70**, 774 (1993).
[9] M. M. Murnane *et al.*, Science **251**, 531 (1991).
[10] J. D. Kmetec *et al.*, Phys. Rev. Lett. **68**, 1527 (1992).
[11] H. Hamster and R. W. Falcone, in *Ultrafast Phenomena VII,* edited by C. B. Harris *et al.*, Springer Series in Chemical Physics Vol. 53 (Springer, New York, 1990).
[12] H. Hamster *et al.*, Phys. Rev. Lett. **71**, 2725 (1993).
[13] J. A. Stamper and B. H. Ripin, Phys. Rev. Lett. **34**, 138 (1975).
[14] J. A. Stamper, Laser Part. Beams **9**, 841 (1991).
[15] C. E. Clayton *et al.*, Phys. Rev. Lett. **70**, 37 (1993).
[16] D. H. Auston and M. C. Nuss, IEEE J. Quantum Electron. **QE-24**, 184 (1988).
[17] D. Grischkowsky *et al.*, J. Opt. Soc. Am. B **7**, 2006 (1990).
[18] P. R. Smith, D. H. Auston, and M. C. Nuss, IEEE J Quantum Electron. **QE-24**, 255 (1988).
[19] X. C. Zhang *et al.*, Appl. Phys Lett. **56**, 1011 (1990).
[20] J. T. Darrow *et al.*, Opt. Lett. **15**, 323 (1990).
[21] D. You *et al.*, Opt. Lett. **18**, 290 (1993).
[22] H. Hamster, Ph.D. thesis, University of California at Berkeley, 1993 (unpublished), available from University Microfilms, Inc., 300 North Zeeb Road, Ann Arbor, MI 48106-1346.
[23] T. W. B. Kibble, Phys. Rev. **150**, 1060 (1966).
[24] T. E. Glover *et al.* (unpublished).
[25] B. M. Penetrante and J. N. Bardsley, Phys. Rev. A **43**, 3100 (1991).
[26] J. D. Jackson, *Classical Electrodynamics,* 2nd ed. (Wiley, New York, 1975).
[27] R. Fedele, U. de Angelis, and T. Katsouleas, Phys. Rev. A **33**, 4412 (1986).
[28] L. Spitzer, *Physics of Fully Ionized Gases* (Wiley, New York, 1962).
[29] Y. R. Shen, *The Principles of Nonlinear Optics* (Wiley, New York, 1984).
[30] A. Sullivan *et al.*, Opt. Lett. **16**, 1406 (1991).
[31] B. I. Greene *et al.*, Appl. Phys. Lett. **59**, 893 (1991).
[32] T. Katsouleas and W. B. Mori, Phys. Rev. Lett. **61**, 90 (1988), and references therein.
[33] A. Sullivan *et al.* (unpublished).
[34] N. G. Basov, Kvant. Elektron. (Moscow) **1** (1), 4 (1971) [Sov. J. Quantum Electron. **1**, 2 (1971)].
[35] G. Mourou, C. V. Stancampiano, and D. Blumenthal, Appl. Phys. Lett. **38**, 470 (1981).
[36] M. J. Berger and S. M. Seltzer, *Stopping Powers and Ranges of Electrons and Positrons* (National Bureau of Standards, Washington, DC, 1982).
[37] R. Fedosejevs *et al.*, Appl. Phys. B **50**, 79 (1990).
[38] N. A. Dyson, *X-Rays in Atomic and Nuclear Physics,* 2nd ed. (Cambridge University Press, Cambridge, 1990).
[39] Q. Heitler, *The Quantum Theory of Radiation,* 3rd ed. (Clarendon, Oxford, 1954).

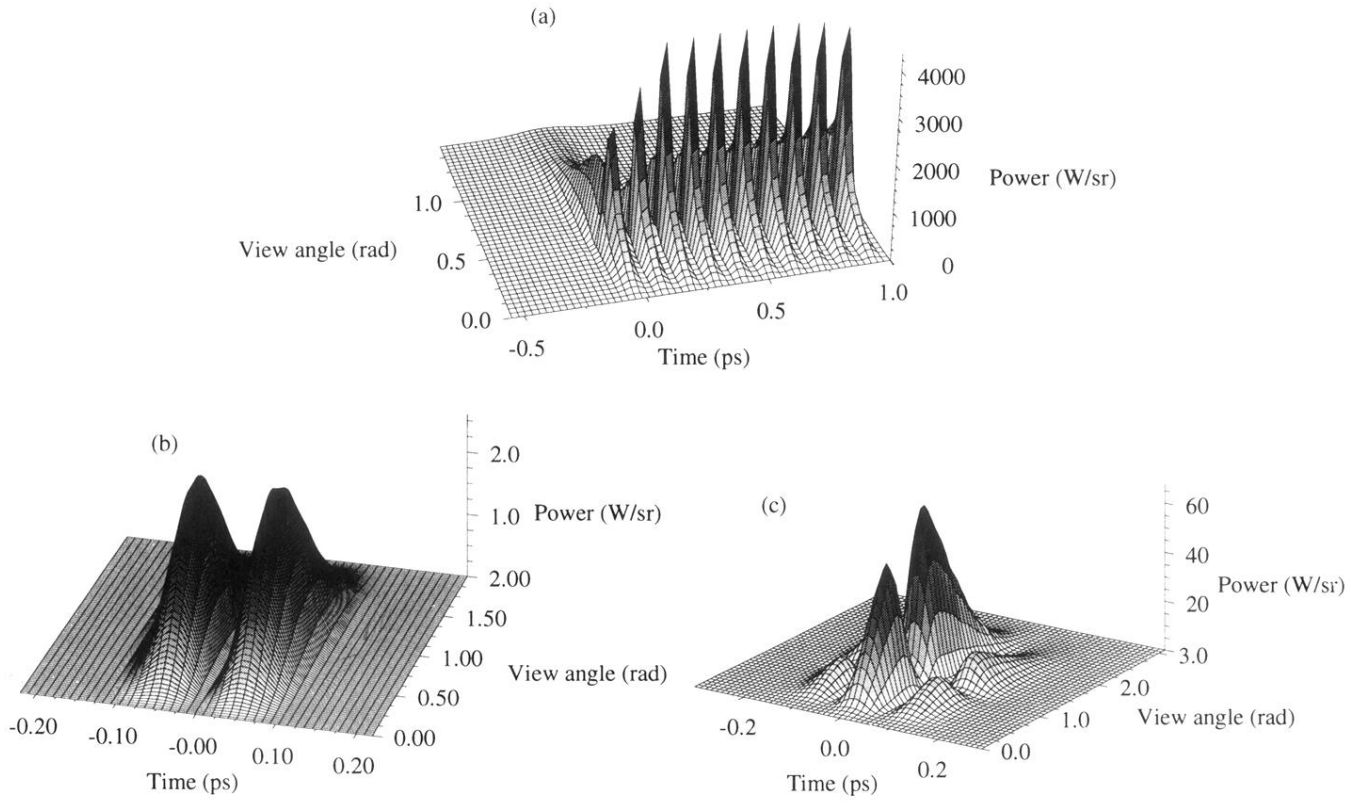

FIG. 1. Calculated radiation pattern. The vertical axis denotes power (W/sr); the bottom axes are time (ps) and view angle (rad) with respect to the beam propagation direction. The calculations are for a pulse length of 120 fs FWHM, 50-mJ pulse energy, and a beam diameter of 3 μm. (a) Resonant plasma response when the electron density is 2.5×10^{17} cm^{-3}. (b) Nonresonant response at a density of 10^{19} cm^{-3}. (c) FIR signal due to $\mathbf{J}^{\mathrm{NL}}$ at a density of 10^{19} cm^{-3}.